Utilization of High-Resolution Boundary Layer Radar and Wavelet to Detect Microscale Downdraft-Updraft Combination

AUTHOR(S):

Nugroho, Ginaldi Ari; Yamaguchi, Kosei; Nakakita, Eiichi; Yamamoto, Masayuki K.; Kawamura, Seiji

CITATION:

Nugroho, Ginaldi Ari ...[et al]. Utilization of High-Resolution Boundary Layer Radar and Wavelet to Detect Microscale Downdraft-Updraft Combination. SOLA 2021, 17: 63-68

ISSUE DATE:

2021

URL:

http://hdl.handle.net/2433/274487

Utilization of High-Resolution Boundary Layer Radar and Wavelet to Detect Microscale Downdraft-Updraft Combination

Ginaldi Ari Nugroho[1], Kosei Yamaguchi[2], Eiichi Nakakita[2],
Masayuki K. Yamamoto[3], and Seiji Kawamura[3]
[1]*Graduate School of Engineering*, *Kyoto University*, *Kyoto*, *Japan*
[2]*Disaster Prevention Research Institute*, *Kyoto University*, *Kyoto*, *Japan*
[3]*National Institute of Information and Communications Technology*, *Tokyo*, *Japan*

Abstract

High-resolution boundary layer radar (BLR) and wavelet are utilized to observe microscale downdraft-updraft combinations. High-resolution BLR can observe thermal activity that pushed the stable layer. During this thermal, a combination of downdraft-updraft was also observed. A detailed observation of this combination was conducted in this study. Using a 1-dimensional continuous wavelet transform with Paul wavelet, we could quantify this downdraft-updraft combination based on the height and period. Using this quantification and wavelet variance in different weather conditions, we showed the essential period from 0 to 0.25 min, 2 to 4 min, and 4 to 8 min of this microscale downdraft-updraft combination.

(**Citation**: Nugroho, G. A., K. Yamaguchi, E. Nakakita, M. K. Yamamoto, and S. Kawamura, 2021: Utilization of high-resolution boundary layer radar and wavelet to detect microscale downdraft-updraft combination. *SOLA*, **17**, 63−68, doi:10.2151/sola.2021-010.)

1. Introduction

While updrafts play an essential role in transporting momentum, energy, and mass from the surface into the atmosphere, downdraft also has a unique role in the atmospheric process. The downdraft in the lower troposphere can increase the possibility of low-level convergence that could enhance another convective development (Kain 2004). Downdraft also has an impact on the production of vertical vorticity at the ground level. A mesoscale simulation showed that the downward parcel changes its orientation under high pressure and then produces vertical vorticity (Parker and Dahl 2015). This vertical vorticity is important because a pair of positive and negative vertical vorticity in the cumulonimbus cloud can indicate a localized heavy rainfall occurrence (Nakakita et al. 2017).

A combination of updraft - downdraft process could generate by thermal forcing of solar heating, vertical wind shear, and also its combination (Huang et al. 2020). Previous studies using numerical simulation showed that updraft-downdraft generated by thermal have a temporal scale of less than a few minutes and a vertical scale of less than 100 m (Yamaguchi et al. 2019).

Another possible combination is the reversed downdraft-updraft process. In mesoscale phenomena, an additional downdraft-updraft circulation is essential for recharging and maintaining the cycle of energy, mass, and moisture budgets in the atmospheric boundary layer and developing new deep convective elements (Gray 2012). In microscale studies, this reversed downdraft-updraft process is still relatively unknown and difficult to observe due to the absence of a high-resolution instrument to observe this kind of combination.

This study aims to verify the existence of the microscale downdraft-updraft process within a certain height during the summer season in the urban area of Kobe, Japan. Another goal is to analyze the microscale downdraft-updraft structure in different weather conditions (clear sky, cloudy, and convective). A detailed explanation of the methodology is provided in the next section. An advanced Boundary Layer Radar (BLR) is introduced to measure vertical wind velocity with high temporal and vertical resolution. The wavelet method is also utilized to determine the downdraft-updraft structure from vertical wind velocity observed by BLR.

2. Methodology

2.1 Dataset

Wind profiler radar is utilized in several applications, such as measuring a vertical profile of horizontal wind for numerical weather prediction (Ishihara et al. 2006; Liu et al. 2020) and observing severe turbulence in the surface wind at the airport (Hisscott 2019). In this study, an advanced BLR with different performance compared with other wind profile radar is used. This advanced BLR can gain a high-resolution vertical profile of vertical wind velocity in the lower atmosphere.

The BLR was installed in an urban area of Kobe, Japan. Coordinate of the location is 34°39′56.87″N and 135°8′34.66″E with elevation 47 meters above mean sea level. Distance from the nearest coastline is 2.24 km, which is on the south side of BLR location. This instrument is equipped with range imaging (RIM) and oversampling (OS) capabilities. RIM with OS is a technique for enhancing the vertical resolution. RIM with OS can resolve vertical wind perturbations with a vertical scale as small as 100 meters (Yamamoto et al. 2014).

This BLR also has the capability of adaptive clutter suppression (ACS). ACS is a technique for mitigating clutter contamination in the received signal (Yamamoto et al. 2017). ACS system composed of three subarray antennas was installed in the BLR. This subarray antenna was designed to be omnidirectional in a horizontal plane to detect clutter existing on or near the ground. Echo power and vertical wind velocity collected by the BLR are used in this study. Both of them are collected with a range sampling of 30-m intervals and a time interval of 8.192 s to resolve small-scale vertical wind variations. BLR specification and observation parameters are briefly described in Tables 2 and 3, respectively. The comparison between advanced BLR with conventional wind profile radar (WPR) is that WPR is not equipped with the setting mentioned above. The disadvantage of advanced BLR is the reduced Nyquist speed and the decrease of Signal to Noise Ratio, although, in this study, this weakness is not affected the data analysis.

2.2 Weather condition classification

The data are then classified into three weather conditions; clear sky, cloudy, and convective condition. In this study, convective is related to dry convective conditions depicted by several clouds existing without precipitation above the BLR during the study period. A time-lapse camera and Himawari-8 satellite (Fig. 1) are used to confirm these classifications conditions. A time-lapse camera that points upward and records cloud image every five seconds is placed in the BLR location. Cloud albedo from band 03

Corresponding author: Ginaldi Ari Nugroho, Graduate School of Engineering, Kyoto University, Gokasho, Uji, Kyoto 611-0011, Japan. E-mail: ginaldi.nugroho.54s@st.kyoto-u.ac.jp.

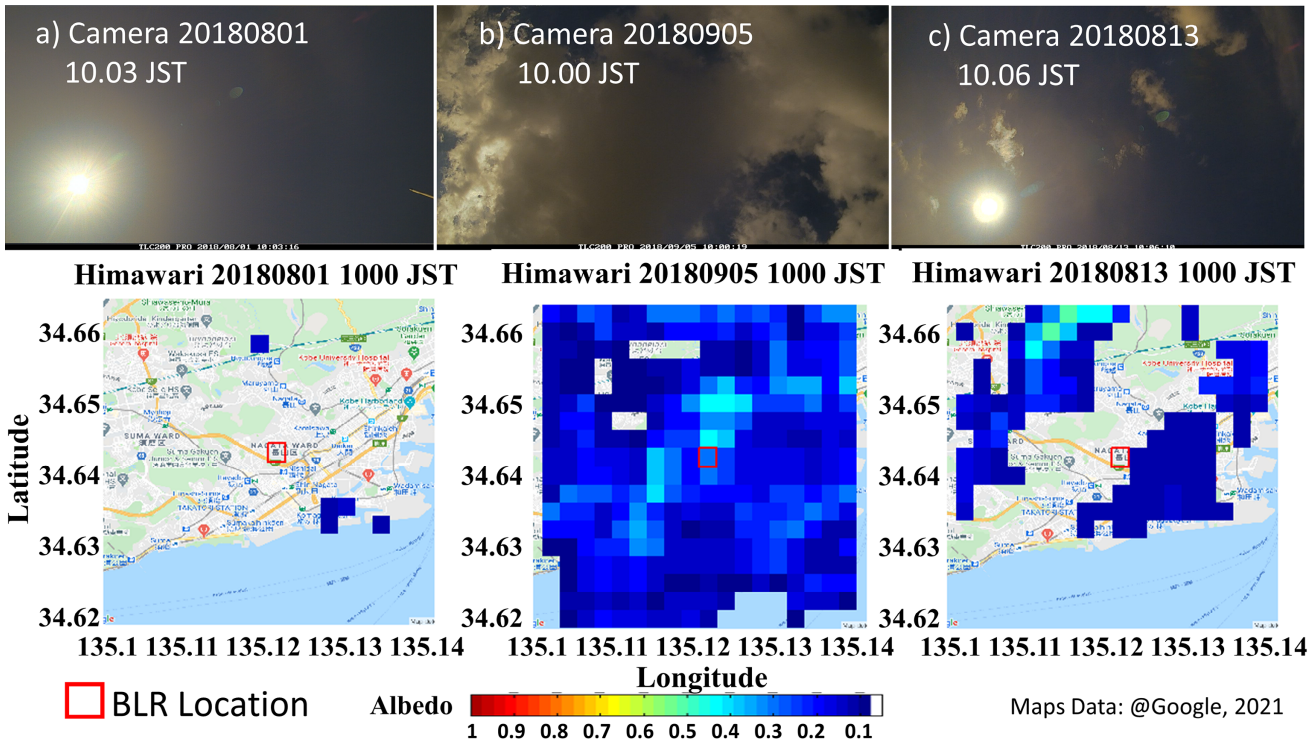

Fig. 1. Example of three weather classification based on time-lapse camera and Himawari albedo. The classified results are (a) clear sky, (b) cloudy, and (c) convective conditions. The upper panels show the image from a time-lapse camera, and the lower panels show the albedo from Himawari-8. Red boxes represent the area where BLR is located.

Table 1. Classification of weather conditions and wind properties from MSM.

Date	Classification	MSM							
		06 JST		09 JST		12 JST		15 JST	
		Dir	Spd	Dir	Spd	Dir	Spd	Dir	Spd
20180718	Convective	SSW	0.83	SSE	0.34	SE	0.55	WSW	0.64
20180719	Clear sky	E	0.63	ESE	0.75	ESE	0.41	SE	1.44
20180723	Convective	E	1.34	S	0.67	SSW	1.00	S	1.88
20180801	Clear sky	SSW	1.43	SSE	1.59	WSW	1.88	SW	2.44
20180804	Clear sky	E	2.07	W	0.46	SSE	1.14	S	1.15
20180813	Convective	ESE	1.31	E	1.20	SW	1.41	SW	1.97
20180830	Cloudy	W	1.43	WSW	1.53	WSW	1.97	W	2.58
20180905	Cloudy	SSE	1.4	SSW	2.26	SW	2.65	SW	2.3
20181013	Cloudy	SW	2.6	SW	1.1	WSW	1.2	S	0.5

Dir = wind direction Spd = wind speed (m/s) Height level = 1000 hPa

of Himawari-8 satellite (Shang et al. 2017) is used to confirm the cloud condition above BLR. Horizontal wind near BLR location from Meso-Scale Model (MSM) is also used as a supporting variable of wind direction and speed. This study period is from 05:00 JST to 16:00 JST within nine selected days from July until October 2018. This period is chosen because the probability of convection is highest due to sunshine duration. The weather classification and wind properties are shown in Table 1. Although wind shear is not considered in this study, environment wind was mostly southerly or southwesterly from Table 1.

2.3 Continuous wavelet transform

A wavelet transform is used to distinguish the downdraft-updraft structure from the vertical wind velocity data. The wavelet transform gives time-frequency information simultaneously for non-stationary time series data (Terradellas et al. 2001). The wavelet transforms absolute squared value is the wavelet power spectrum that expressed the correlation information between the wavelet function and the time series data. In this study, continuous wavelet transform (CWT) is used because of its ability to extract particular characteristics (Wiebe et al. 2011). CWT applications are based on Torrence and Campo (1998) algorithm, which is expressed as follows.

$$W_n(s) = \sum_{n'=0}^{N-1} X_{n'} \Psi^* \left[\frac{(n'-n)\delta t}{s} \right] \quad (1)$$

where $X_{n'}$ is the data of vertical wind velocity time series, N is the length of the data, Ψ^* is the complex conjugate of the wavelet function, δt is the sampling interval, and s is the wavelet scale. It is necessary to define the scale and determine the smallest (s_0) and largest (s_j) resolvable values of the scale, the number of scales used (j), and also its interval (δj). Equation (2) is used to determine the scale with a convenient scale as a power fraction of two.

$$s_j = s_0 2^{j\delta j} \quad (2)$$

$$j = (\log_2(N\delta t / s_0))/\delta j \quad (3)$$

Wavelet is calculated in the unit of minutes. The δt is achieved by calculating the amount of BLR data in one minute and then

Table 2. Boundary layer radar specification.

Frequencies	
Center Frequency	1357.4 MHz
Maximum Number	5
Switch mode	Pulse-to-pulse basis
Main Antenna	
Type	Active phased array antenna composed of 7 Luneberg lenses
Gain	29.6 dBi
3-dB beam width	5.1°
Beam Direction (Azimuth, Zenith)	(0°, 0°), (0°, 14°), (90°, 14°), (180°, 14°), (270°, 14°)
Transmitter	
Peak Power	2.8 kW
Pulse Compression	Phase-modulation using binary codes
Receiver	
Noise Figure	1.7 dB
Gain	> 70 dB
Digital Phase Detection	Executed by the ACS System (Yamamoto et al. 2017)
Real-time Signal Processing	Executed by the ACS System (Yamamoto et al. 2017)
Location	
Latitude	34°39′57″N
Longitude	135°08′35″E
Sea Level Altitude	45 m

Table 3. Observation parameter.

Frequencies	1356.65 MHz 1357.00 MHz 1357.40 MHz 1357.75 MHz 1358.15 MHz
Transmitted Pulse Compression	Spano code (8 bit, 16 sequences)
Sub Pulse Width	1 μs
Inter Pulse Period	50 μs
Sample Start Range	300 m
Sampling Interval	0.2 μs
Number of Sampled Points in Range	180
Number of Time Series Points	512
Collection Interval for Vertical Beam	4.096 s (2.048 s for vertical beam and 2.048 s for oblique beam)
Nyquist Velocity	13.8 m/s
Horizontal Extent of Vertical Beam (at Height of 1 km)	62.9 m
Maximum Observation Range (Altitude)	5715 m

dividing it by how many minutes in 11 hours (05:00−16:00 JST). The calculated δt is 0.0111. Then, using Eqs. (2) and (3) resulted in the s_0 and s_j value of 0.0444 and 46, respectively. The number of wavelet scales used is 41 scales. Scale period is calculated from the wavelet scale multiplied by Fourier factors that depend on the type of mother wavelet used (Torrence and Campo 1998). The smallest scale period used is 0.25 min because it needs a minimum of two data to capture the downdraft-updraft combination.

Next, an appropriate mother wavelet is chosen. A detailed process of choosing a mother wavelet will be discussed in Section 3. The cone of influence (COI) region is applied by padding the end of the time series with zeroes before repeating the wavelet transform cycle. COI is used to separate the wavelet power spectrum from unrelated values due to the decrease in wavelet power. Calculating a significant wavelet power spectrum that has values above the background spectrum is needed to distinguish the target real physical feature (Torrence and Campo 1998). The most significant value is then overlaid on the wavelet power spectrum in the form of a marked black region. Quality control is conducted by checking the significant value of the wavelet power spectrum and comparing them with the downdraft-updraft time series to verify that only the downdraft-updraft signature is collected.

Another constraint that needs to be considered is the missing data from BLR product. Wavelet is unable to calculate a missing data or non-number value. Meanwhile, in the BLR observation, it is common to have an increased number of missing data throughout the height. Due to that reason, the wavelet calculation is only focused on range height from 300 m to 1500 m. Nearest-neighbor interpolation is also used to handle the rest of the missing data that still exist.

3. Results and discussion

3.1 Fine structure of downdraft-updraft from BLR

Figure 2 shows an example of the data on 23 July 2018 from 09:00 to 10:00 am JST. Figure 2b showed two significant updrafts; the first was at 09:17 JST and the second was at 09:25 JST, where the first updraft was not as strong as the second. Between these two updrafts, a strong downdraft occurred, lasting approximately 5 min at the height of 400−700 m. The second updraft seemed to push the stable layer observed above the enhanced echo power (Figs. 2a and 2b).

A combination of the downdraft and the second updraft (downdraft-updraft) was observed below a height of 1100 m. The changing value of this downdraft-updraft combination started from a height of 500 m. Figure 2b shows this fine structure in a high temporal and vertical aspect, which revealed the advanced BLR high performance. The coherent structure of the second updraft is not affected by the horizontal wind at the surface (Fig. 2c), which is likely due to the weak horizontal wind during that period.

The wavelet method was applied to determine this type of downdraft-updraft pattern. The wavelet method is applied to the vertical wind velocity, and two main tasks need to be considered. The first task is to determine a method for distinguishing this downdraft-updraft pattern from other fluctuation patterns. The second task is to determine the characteristics of this structure under different conditions.

3.2 Wavelet method

a. Choosing mother wavelet

A wavelet is applied to the data to distinguish the downdraft-updraft pattern. Figure 2 demonstrates that the form of downdraft-updraft exists from 500 to 1100 m as the target. Once the target is determined, the analysis can start using different mother wavelets and choosing the appropriate one.

Three different types of mother wavelets (Morlet wavelet, Paul wavelet, Mexican hat wavelet) were utilized via 1-dimensional CWT (CWT-1D) and applied to the same data in Fig. 2b only from height 500−1100 m, with the result is shown in Fig. 3. The downdraft-updraft target is marked in the red dashed box. The wavelet power spectrum results using the Morlet wavelet, Paul wavelet, and Mexican hat wavelet is marked in blue, black, and green dashed boxes. Different shapes of each mother wavelet (in the time domain) are also added in the dashed boxes upper part.

In Fig. 3, the signature that represents the target (downdraft-updraft combination) is shown in the marked black region. This result showed that the Morlet and Paul wavelets could identify the distinctive form of a downdraft-updraft combination. In contrast, the Mexican hat wavelet could not identify the downdraft-updraft combination because the Mexican hat tends to separate the downdraft and updraft. This characteristic is likely because the Mexican hat wavelet only calculates the real value. Meanwhile, the phase shift from downdraft and updraft is in complex value (De Moortel et al. 2004). Therefore, the Mexican hat wavelet was not used in this data analysis.

A detailed comparison between the Morlet and Paul wavelets showed that the Paul wavelet has a better signature pattern with a narrow shape throughout the time (horizontal axis), especially at the height between 500 and 700 m. This characteristic means that the Paul wavelet could detect the very localized combination of downdraft-updraft. Another difference is the height of the signature in the scale period (vertical axis), where the Paul wavelet showed a much taller shape compared with the Morlet wavelet.

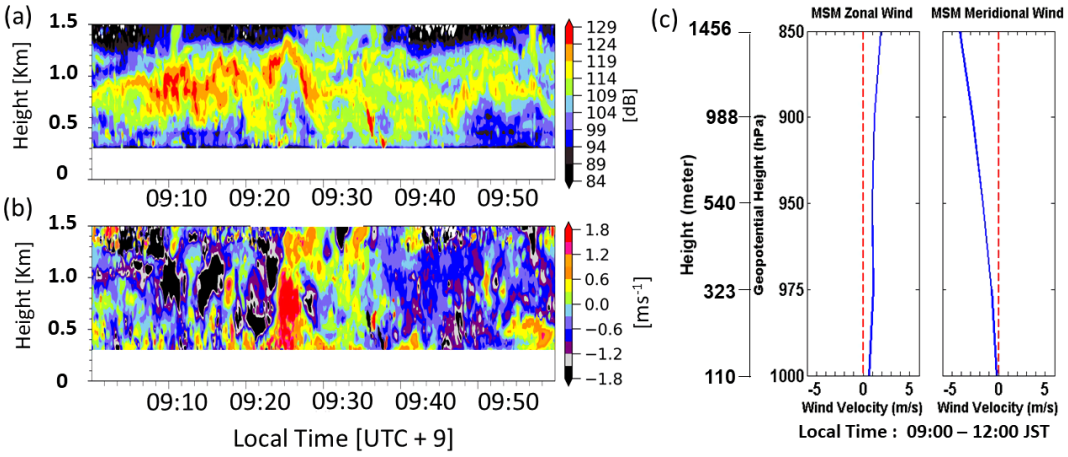

Fig. 2. The time-height plot of (a) echo power and (b) vertical wind velocity measured by the BLR from 09:00 to 10:00 JST on 23 July 2018. (c) Vertical profile of MSM wind velocity during 09:00−12:00 JST on 23 July 2018. A positive value in vertical wind velocity represents updraft, while a negative value represents downdraft. The lowest height of echo power and that of vertical wind velocity are 300 m.

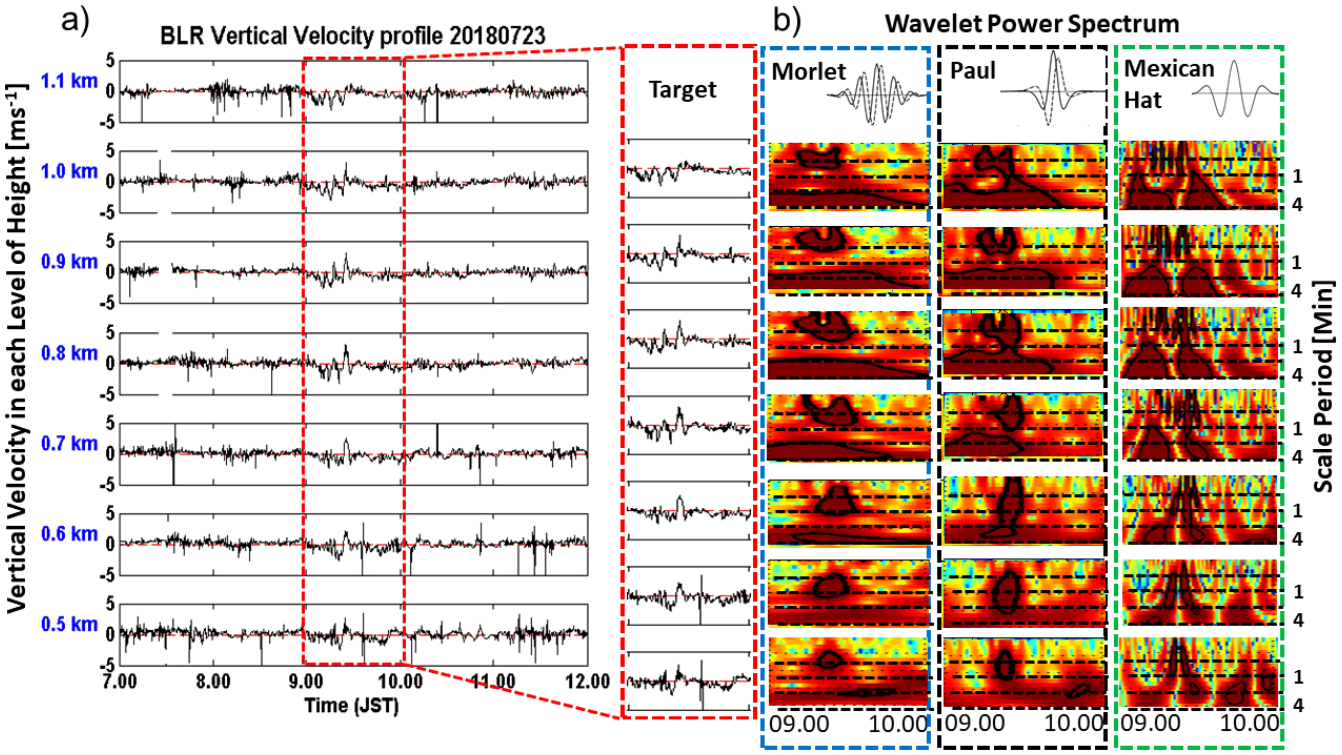

Fig. 3. Comparison of the wavelet results using different mother wavelets. (a) Time series of vertical wind velocity. Red boxes show the target downdraft-updraft signal. (b) Wavelet results from each height of the target signal with different mother wavelets. See text for details of the mother wavelets.

This characteristic is correlated with the mother wavelet shape characteristic, where the Paul wavelet has less oscillation than the Morlet wavelet. A smaller number of oscillations will yield a very accurate time resolution but reduce the frequency resolution (De Moortel et al. 2004). This study is using paul wavelet considering its better signature pattern and less oscillation.

b. Downdraft-updraft structure identification

CWT 1D with the Paul wavelet is then applied to the data, with one example is in Fig. 4 on 23 July 2018. Two criteria are used to define the downdraft-updraft structure; 1) wavelet power spectrum signature with a 95% confidence level marked by a thick enclosed region and 2) the signature must be located inside the COI area separated by a dashed black line. Based on these criteria, a signature of the downdraft-updraft structure can be collected.

Figure 4a shows a time variation of the vertical wind velocity at the height of 480 m. An example of the distinctive downdraft-updraft signature was detected from approximately 09:00 to 10:00 JST. The wavelet power spectrum in Fig. 4b also shows a significant signature that conforms with these two criteria (thick enclosed region and COI).

Several thick enclosed signatures also appeared at various time occurrences and periods. The signatures are then counted on each scale period in every height with an increment of 90 m. This counted signature is defined in this study as the number of occurrences. The number of occurrences in three different conditions (convective, clear sky, cloudy) is analyzed to observe the characteristics to achieve more reliable results.

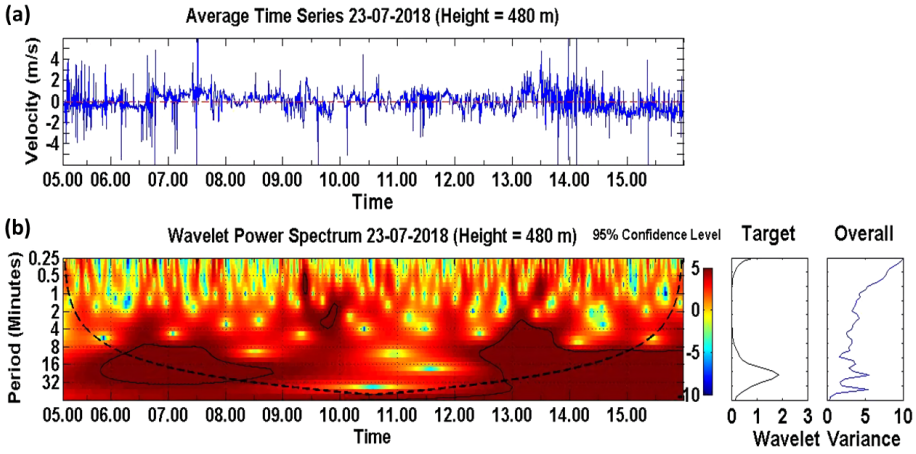

Fig. 4. Wavelet result example using a Paul wavelet on 23 July 2018 at the height of 480 m. (a) Time variation of the vertical wind velocity and (b) wavelet power spectrum. The dashed line in Fig. 4b is the COI, and the marked black curve is the downdraft-updraft signature extracted by a 95% confidence level. The panel on the right side of (b) is the wavelet variance on each period of the downdraft-updraft signature and overall wavelet power spectrum, respectively.

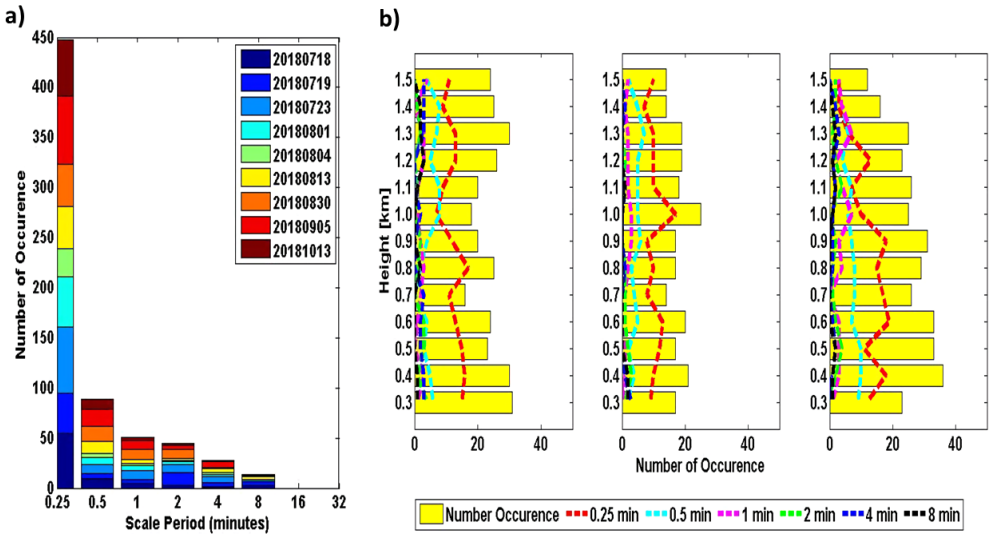

Fig. 5. Downdraft-updraft number of occurrences, (a) based on period, (b) based on height. Figure 5b shows that only six scales of 0.25, 0.5, 1, 2, 4, and 8 min are shown.

3.3 Characteristic downdraft-updraft

The two main results of the number of occurrences are based on the scale period and height. This study classified the period into eight classifications (0.25, 0.5, 1, 2, 4, 8, 16, 32 min). This period means the estimated duration of the downdraft-updraft combination based on the wavelet calculation. The quantified number of occurrences based on the period is shown in Fig. 5a. The occurrences in all the weather conditions are counted. There are six periods from this classification that have more value, that is 0.25, 0.5, 1, 2, 4, and 8 min. The period of 0.25 min is dominant than other periods. This probably because most of the downdraft-updraft combinations are occurring in a short duration.

Figure 5b shows the total number of occurrences at each height represent by the yellow bar. This figure demonstrates that the maximum value in the convective and cloudy conditions is observed at a lower height of approximately 300 m and 400 m. Meanwhile, the colored line showed the six periods. As expected, the red curve (0.25 min period) is dominant within others. In cloudy conditions, the red curve is decreasing along with the height.

Further analysis of the structure at six different scale periods using wavelet variance is shown in Fig. 6. Wavelet variance is conducted by calculating a variance from the significant wavelet power spectrum over time series. This wavelet variance is showed in three different conditions (convective, clear sky, and cloudy) at three height classification (lower: 300−480 m, middle: 510−1020 m, and upper:1050−1500 m), with maximum scale period limited until 8 min refer to the result in Fig. 5a.

Figure 6 showed that variance is more significant in the upper level in all weather conditions. In clear sky conditions, the variance is less than other conditions (convective and cloudy). There are distinctive patterns in clear sky condition in scale period 0−0.25 min and 2−4, 4−8 min. In the convective condition, this distinctive pattern more and more apparent in each height classification.

The similar pattern of downdraft-updraft along the height in the convective condition can be classified into two types: the characteristics of downdraft-updraft are always similar, the other is that the downdraft-updraft went upward for a long distance of height so that the same downdraft-updraft showed less variance. Further analysis is required to solve this problem.

Figures 5 and 6 showed that the period suitable for the downdraft-updraft combination behavior is the 0−0.25 min, 2−4 min, and 4−8 min period in this study. The wavelet method using Paul wavelet applied in the data can distinguish and calculate the downdraft-updraft combination. This method could help understand the downdraft-updraft behavior, especially in the convective condition, after evaluation through many events.

4. Conclusion

This paper described the advanced BLR ability to observe a combined downdraft-updraft structure around the thermal. CWT 1D is utilized to quantify and analyze the characteristics of this combined downdraft-updraft structure. The use of different mother wavelets and scales were compared to obtain a suitable detection of the combined downdraft-updraft structure. Vertical wind

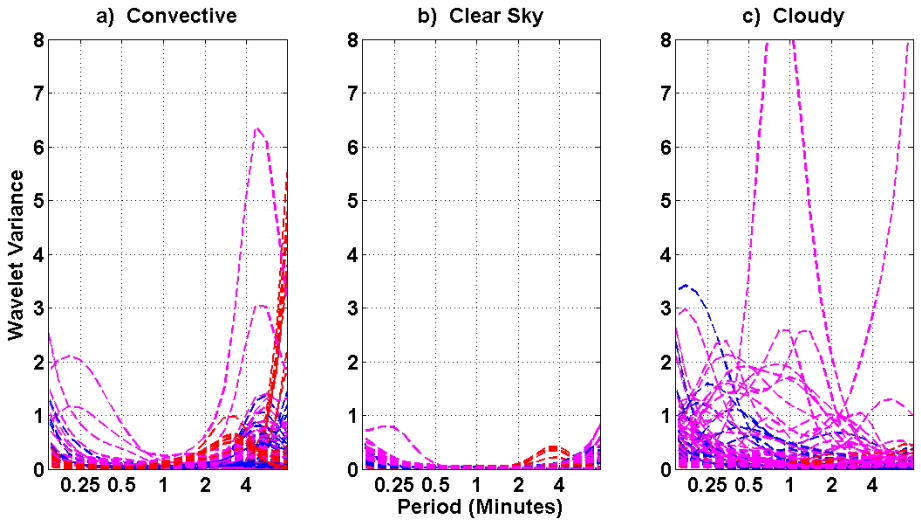

Fig. 6. Wavelet variances based on scale periods from height 300 m to 1500 m in different weather conditions of (a) convective, (b) clear sky, and (c) cloudy. Red lines represent the variance in lower height (300 to 480 m), blue lines represent the variance in middle height (510 to 1020 m), and magenta lines represent the variance in upper height (1050 to 1500 m).

velocity measured by the advanced BLR in three different weather conditions is then examined using CWT 1D based on scale and height. The quantified number of occurrence and wavelet variance showed that the downdraft-updraft structure has a suitable period from 0 to 0.25 min, 2 to 4 min, and 4 to 8 min. Detailed analysis of the variance in every height is needed in future studies.

An appropriate mother wavelet combined with vertical wind velocity from high-resolution BLR can identify the downdraft-updraft combination on a nine-day dataset (different weather conditions) in this study. This technique added with analysis of both power spectrum and variance could determine the period and quantified the number of occurrences. This information is essential for understanding the downdraft-updraft behavior related to the boundary layer microscale condition, especially in convective conditions.

Acknowledgments

This work was supported by JSPS KAKENHI, Grant Numbers 15H05765, 20H02258, 16K12861. The author would also thank the Indonesia Endowment Fund for Education (LPDP) for supporting his study.

Edited by: H. Hashiguchi

References

De Moortel, I., S. A. Munday, and A. W. Hood, 2004: Wavelet analysis: The effect of varying basic wavelet parameters. *Solar Physics*, **222**, 203−228.

Gao, W., and B. L. Li, 1993: Wavelet analysis of coherent structures at the atmosphere-forest interface. *J. Appl. Meteor.*, **32**, 1717−1725.

Gray, W. M., 2012: Fundamental importance of convective downdrafts and mass recycling within the tropical cloud cluster and the typhoon-hurricane. *Trop. Cycl. Res. Rev.*, **1**, 130−141.

Hisscott, A., 2019: Exploiting wind profiler information. *Weather*, **74**, 8−19.

Huang, T., S. H. L. Yim, Y. Yang, O. S. M. Lee, D. H. Y. Lam, J. C. H. Cheng, and J. Guo, 2020: Observation of turbulent mixing characteristic in the typical daytime cloud-topped boundary layer over Hng Kong in 2019. *Remote Sens.*, **12**, 1533.

Ishihara, M., Y. Kato, T. Abo, K. Kobayashi, and Y. Izumikawa, 2006: Characteristics and performance of the operational wind profiler network of the Japan Meteorological Agency. *J. Meteor. Soc. Japan*, **84** , 1085−1096.

Kain, J. S., 2004: The Kain–Fritsch convective parameterization: an update. *J. Appl. Meteor.*, **43**, 170−181.

Liu, B., J. Guo, W. Gong, L. Shi, Y. Zhang, and Y. Ma, 2020: Characteristics and performance of wind profiles as observed by the radar wind profiler network of China. *Atmos. Meas. Tech.*, **13**, 4589−4600.

Nakakita, E., H. Sato, R. Nishiwaki, H. Yamabe, and K. Yamaguchi, 2017: Early detection for baby-rain-cell aloft in a severe storm and risk projection for urban flash flood. *Adv. Meteor.*, doi:10.1155/2017/5962356.

Parker, M. D., and J. M. Dahl, 2015: Production of near-surface vertical velocity by idealized downdraft. *Mon. Wea. Rev.*, **143**, 2795−2816, doi:10.1175/MWR-D-14-00310.1.

Shang, H., L. Chen, H. Letu, M. Zhao, S. Li, and S. Bao, 2017: Development of a daytime cloud and haze detection algorithm for Himawari-8 satellite measurements over central and eastern China. *J. Geophys. Res. Atmos.*, **122**, 3528−3543.

Terradellas, E., G. Morales, J. Cuxart, and C. Yagüe, 2001: Wavelet methods: Application to the study of the stable atmospheric boundary layer under non-stationary conditions. *Dyn. Atmos. Oceans*, **34**, 225−244.

Torrence, C., and G. P. Campo, 1998: A practical guide to wavelet analysis. *Bull. Amer. Meteor. Soc.*, **79**, 61−78.

Wiebe, A., A. Sturman, and H. McGowan, 2011: Wavelet analysis of atmospheric turbulence over a coral reef flat. *J. Atmos. Oceanic Technol.*, **28**, 698−708.

Yamaguchi, K., T. Tsuchihashi, and E. Nakakita, 2018: Analysis of the formation of vortex tube and thermals above urban area by urban meteorological model based on large eddy simulation. *DPRI Annuals*, 62B.

Yamamoto, M. K., S. Kawamura, and K. Nishimura, 2017: Facility implementation of adaptive clutter suppression to an existing wind profiler radar: First result. *IEICE Commun. Exp.*, **6**, 513−518, doi:10.1587/comex.2017XBL0075.

Yamamoto, M. K., T. Fujita, N. H. B. A. Aziz, T. Gan, H. Hashiguchi, T. Y. Yu, and M. Yamamoto, 2014: Development of a digital receiver for range imaging atmospheric radar. *J. Atmos. Sol.-Terr. Phys.*, **118**, 35−44, doi:10.1016/j.jastp.2013.08.023.

Manuscript received 9 December 2020, accepted 3 February 2021
SOLA: *https://www.jstage.jst.go.jp/browse/sola/*